Central peaks, acoustic modes, and the dynamics of polar nanoregions in $Pb[(Zn_{1/3}Nb_{2/3})_xTi_{1-x}]O_3$ single crystals studied by Brillouin spectroscopy

Jae-Hyeon Ko*
Department of Physics, Hallym University, 39 Hallymdaehakgil, Chuncheon, Gangwondo 200-702, Korea

Do Han Kim and Seiji Kojima*
Institute of Materials Science, University of Tsukuba, Tsukuba City, Ibaraki 305-8573, Japan
(Received 2 November 2007; published 12 March 2008)

Temperature dependence of acoustic behaviors and quasielastic central peaks (CPs) of $Pb[(Zn_{1/3}Nb_{2/3})_xTi_{1-x}]O_3$ (PZN-xPT) single crystals with $x=4.5\%$ and 9% have been investigated in a temperature range of 300–900 K by using the Brillouin light scattering. The temperature dependence of the C_{11} elastic constant of both crystals showed a deviation from normal lattice anharmonicity at the Burns temperature (T_B) of about 730 K upon cooling, indicating the onset of the electrostrictive coupling between the polar nanoregions (PNRs) and the longitudinal acoustic (LA) waves. Upon further cooling, depolarized CP began to appear at a certain temperature (T_d) located in 500–550 K, which was accompanied by substantial softening of the C_{44} elastic constant below this temperature suggesting anisotropic electrostrictive coupling between PNRs and the two acoustic waves. In addition, the onset of significant increase in the acoustic damping of both acoustic waves at T_d could be seen from the temperature dependence of the linewidth of Brillouin doublets. These results suggested that electrostrictive coupling of the strain to the square of the local polarization of PNRs and the resultant order-parameter fluctuations are enhanced not at T_B but at a much lower temperature of T_d, which may be ascribed to a local structural transformation occurring in PNRs at T_d. This suggestion is consistent with recent studies on PZN-xPT single crystals reporting the appearance of strong acoustic emission signals [M. Roth *et al.*, Phys. Rev. Lett. **98**, 265701 (2007)] and substantial changes in the Raman spectrum [O. Svitelskiy, Phys. Rev. B **72**, 172106 (2005)] at almost the same temperature. From the comparison of the present results to those of two typical relaxors, $Pb(Mg_{1/3}Nb_{2/3})O_3$ and $Pb(Mg_{1/3}Ta_{2/3})O_3$, it was suggested that the existence of an intermediate characteristic temperature T_d below T_B may be considered as a more common characteristic in the temperature evolution of PNRs of relaxor ferroelectrics.

DOI: 10.1103/PhysRevB.77.104110 PACS number(s): 77.80.−e, 78.35.+c, 77.84.Dy, 77.65.Bn

I. INTRODUCTION

Lead-based perovskite $A(B_{1/2}B'_{1/2})O_3$ and $A(B_{1/3}B'_{2/3})O_3$ relaxor ferroelectrics (RFEs) with $A=Pb$ are a special group of ferroelectric materials that show complex structural and dynamical behaviors.[1,2] RFEs have attracted great attention from the viewpoints of both fundamental physics and applications, since they exhibit extraordinary electromechanical and dielectric properties having wide applications in the field of piezoelectric and pyroelectric devices, high-k capacitors, etc.[3] A typical RFE, for example, $Pb(Mg_{1/3}Nb_{2/3})O_3$ (PMN), shows a diffuse, frequency-dependent broad dielectric maximum in a temperature window,[4] which is in contrast to the normal ferroelectrics which display a frequency-independent sharp, divergent dielectric susceptibility at the phase transition temperature. The frequency dependence of the temperature of the dielectric maximum (T_m) is found to satisfy the phenomenological Vogel-Fulcher relationship, and the distribution of dielectric relaxation times becomes extremely polydispersive with divergent leading edge on cooling.[5] PMN exhibits no macroscopic symmetry change down to the lowest temperature of 5 K maintaining an average cubic structure although a local polar structure with rhombohedral distortion has been revealed by neutron diffraction study.[6] This intrinsic local distortion constitutes the so-called polar nanoregions (PNRs) which begin to appear below a certain temperature. This temperature, which is called Burns temperature (T_B), is typically a few hundred degrees higher than T_m.[7]

One of the key ingredients of relaxor behaviors is the lattice disorder introduced into the perovskite structure by chemical substitution or lattice defects.[8] Chemically ordered nanosized regions (CORs) are formed by the two different cations with dissimilar valence states which occupy the perovskite B sites. Due to the different valance states, these short-range CORs induce charge disorder and thus become the source of quenched random fields in RFEs. Coupling between the random fields and ferroelectric degrees of freedom such as a soft lattice mode has been suggested to generate PNRs at high temperatures. Due to the random directions of polarizations of PNRs, there is no macroscopic polarization without electric bias. However, since the square of the local polarizations of PNRs is not zero, some physical properties coupled to PNRs via electrostriction may show abnormal behaviors when PNRs begin to appear.

The existence of T_B has been evidenced by many unusual properties of RFEs such as the deviation of the dielectric constant from the high-temperature Curie-Weiss law, appearance of diffuse elastic scattering, deviations of the index of refraction, the volume of the cubic cell from high-temperature linear behaviors, etc.[9] In spite of all the experimental and theoretical efforts on relaxors including the random-field model,[10] the dipolar glass model,[4] and the recent spherical random-bond–random-field model,[11] the exact

nature of PNRs and their relation with CORs have remained as one of the central problems of RFEs. Recent first-principles-based simulations on $Pb(Sc_{1/2}Nb_{1/2})O_3$ showed that the characteristic lengthscale for PNRs is the same as for CORs and also that PNRs appear predominantly in these chemical nanoregions.[12] However, it remains to be confirmed whether the compositional heterogeneity is prerequisite to the formation of PNRs since some phenomena typically related to the relaxation of dynamic PNRs, namely, the significant Brillouin quasielastic scattering, the softening of the longitudinal acoustic mode, and the deviation from the Curie-Weiss law above the Curie point were observed in PMN-55%PT where CORs are known to be absent.[13] More thorough experimental efforts are highly needed to find out the origin of PNRs, their growth mechanism, and their relation to CORs.

Recent systematic Raman studies on PMN, $Pb(Zn_{1/3}Nb_{2/3})O_3$ (PZN), and $Pb[(Zn_{1/3}Nb_{2/3})_{1-x}Ti_x]O_3$ (PZN-xPT) with $x=4.5\%$ indicated an existence of some intermediate characteristic temperature, denoted as T_d in this paper, located between T_B and T_m.[14–16] This intermediate temperature is characterized by anomalies in the temperature dependences of frequency and/or intensity of Raman optic modes and low-frequency central peaks (CPs) observed in Raman spectra. T_d has been suggested as the onset temperature of long-lived correlations between off-center ions resulting in the formation of permanent PNRs.[15] Neutron scattering studies suggested a local phase transition in PMN occurring at ~370 K, below which the intensity of the elastic diffuse scattering increases substantially.[17] This result was interpreted in terms of the random-field model and the cubic anisotropy.[18] These results seem to be consistent with that obtained from recent acoustic emission measurement, which showed clear, strong signals near 510 K in PZN and PZN-9%PT in addition to the acoustic emission activity near T_B ~730 K in both components.[19] More interestingly, succeeding studies on PZN-xPT with $x=0-0.12$ by the same group revealed that strong acoustic emission signals were observed in all the investigated crystals at very similar temperatures of 499–508 K, which were attributed to local martensitelike cubic-to-tetragonal ferroelectric transitions occurring in PNRs.[20] It is also worth pointing out that these characteristic temperatures are close to the values at which the temperature-dependent component of the diffuse x-ray scattering intensity begins to grow in PZN-8%PT[21] and also some rhombohedral distortion begins to appear in PZN.[22]

If there is some local structural changes in PNRs near T_d, it should be accompanied by local strain fields around PNRs which may affect elastic properties of RFEs. In this respect, inelastic Brillouin light scattering can be a very useful tool because it can directly probe acoustic modes which can be coupled to the PNRs through electrostrictive coupling. In addition, characteristic time scales of the polarization fluctuations of PNRs, which manifest themselves as CPs in the low-frequency light scattering spectrum, are located in the Brillouin frequency window. The temperature dependence of the relaxation times of PNRs is an important information for the understanding of their dynamics. Previous Brillouin-scattering studies on PZN-x%PT have mainly been focused on the diffuse phase transitions near the dielectric maxima and thus been carried out in limited temperature ranges of which the upper limits are much lower than T_B.[23–29] In addition, detailed polarization analysis on CPs has not been carried out. Therefore, clear correlations between the relaxor dynamics, in particular, the temperature evolution of PNRs and the acoustic properties, could not be discussed. In our previous letter, changes in the acoustic waves and CP behaviors were pointed out at the intermediate temperature of ~550 K in PZN-9%PT.[30] The present contribution reports on more detailed, systematic investigations of the temperature dependence of acoustic modes and CPs of PZN-xPT with $x=0.045$ and 0.9 as well as PMN and $Pb(Mg_{1/3}Ta_{2/3})O_3$ (PMT) in a wide temperature range between 300 and 900 K. Special attention has been given to the correlation between the dynamics of PNRs and changes of acoustic properties of these RFEs in order to find out whether T_d has a real physical meaning in the temperature evolution of relaxor dynamics.

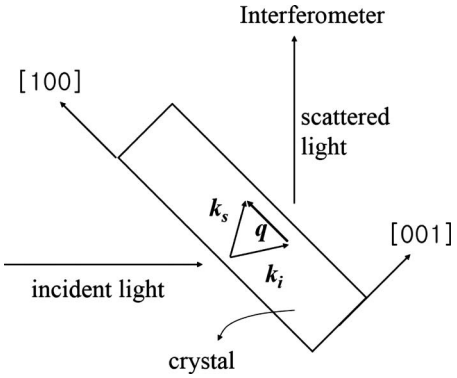

FIG. 1. A right-angle scattering geometry adopted in the present study.

II. EXPERIMENT

PZN-4.5%PT and PZN-9%PT single crystals were grown by using the Bridgman method at the Shanghai Institute of Ceramics. Surfaces were polished to optical quality for light scattering experiments. Pseudocubic crystal orientation was determined using the Laue diffraction pattern. A 3+3 pass tandem Fabry-Pérot interferometer was used to measure the Brillouin spectra of PZN-xPT single crystals. A diode-pumped solid state laser (DPSS532) was used to excite the samples with a wavelength of 532 nm and a power of about 100 mW. Since the elastic scattering is very strong at a backward scattering geometry, a special right-angle scattering geometry was used for the measurement without any significant disturbance of the elastic scattering. Figure 1 shows a schematic diagram of the scattering geometry adopted in the present study. The laser light with a vertical polarization is incident on the (001) surface with an incidence angle of 45°. $\vec{k}_i$ and $\vec{k}_s$ denote the wave vectors of the incident and scattered light, respectively, propagating in the crystal. The phonon propagation direction $\vec{q}$ is thus along the [100] direction. Both the polarized (VV) and depolarized (VH) spectra were obtained during the cooling process by using an analyzer in front of the entrance pinhole of the interferometer. In order to

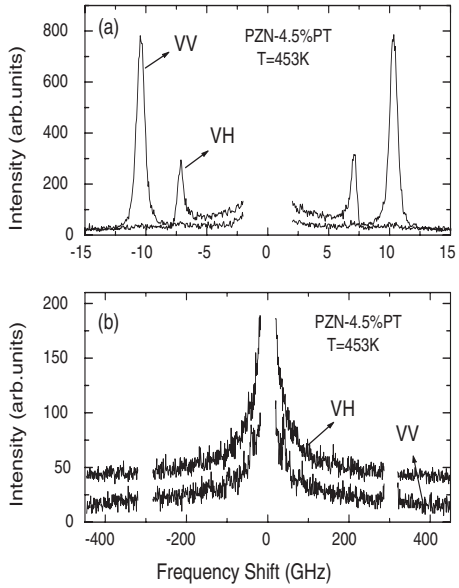

FIG. 2. Polarized (VV) and depolarized (VH) Brillouin spectra of PZN-4.5%PT single crystals measured in (a) narrow and (b) wide frequency ranges at 453 K.

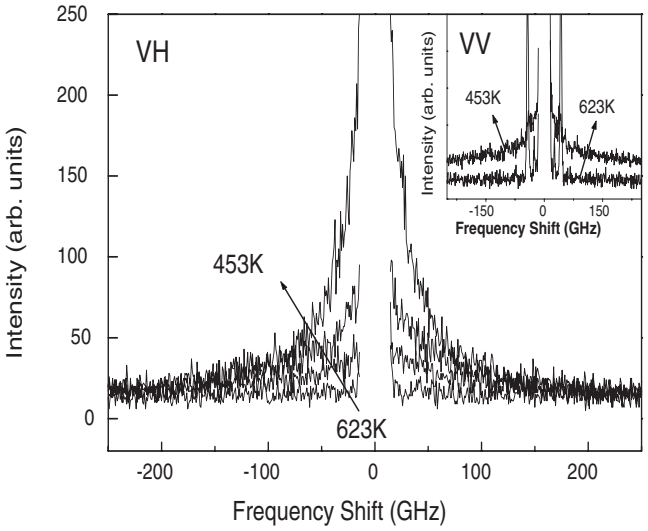

FIG. 3. The depolarized spectrum of PZN-4.5%PT at selected temperatures. The measurement temperatures are 623, 523, 493, and 453 K in sequence. The polarized spectrum is shown in the inset at two temperatures.

cover a wide frequency range for probing CP, a free spectral range of 300 GHz was chosen and a scan range of ±450 GHz was used. A much narrower free spectral range of 20 GHz for scanning ±30 GHz was used for the investigation of acoustic modes. Two elastic stiffness coefficients C_{44} and C_{11} can be obtained in VH and VV scattering geometries, respectively, according to the Brillouin selection rule.[31]

For comparisons of the acoustic properties of PZN-xPT with respect to typical relaxors, the Brillouin spectra of PMN and PMT were measured at the same scattering geometry in a wide temperature range. These crystals were grown by the flux method at the Ioffe Physico-Technical Institute in Russia and prepared in the same way as PZN-xPT single crystals. Both the LA and transverse acoustic (TA) modes were probed and analyzed for comparison. All the above Brillouin experiments were performed at the Institute of Materials Science, University of Tsukuba.

III. RESULTS

A. Brillouin spectra and analysis

Figure 2(a) gives two Brillouin spectra of PZN-4.5%PT single crystals measured at 453 K in a narrow frequency window of ±15 GHz. As can be seen, the TA mode appears in the VH spectrum while the LA mode is shown in the VV spectrum. Similar spectra were also observed in PZN-9%PT.[30] The sound velocities of the TA and LA modes are related to the elastic stiffness coefficients C_{44} and C_{11}, respectively. The CP was investigated in a much wider frequency range of ±450 GHz, and one example of CP spectra at 453 K is plotted in Fig. 2(b). CP of PZN-4.5%PT develops with decreasing temperature and can be seen in both polarized and depolarized geometries at low temperatures below ~550 K. The temperature evolution of CP in both VV and VH geometries can be seen from Fig. 3, which shows that the intensity of CP increases and its width decreases with decreasing temperature down to 453 K. The VH component disappears at high temperatures above 550 K, and the VV component of CP can also hardly be seen at high temperatures above 600 K although a slight slope in the spectrum persists even at much higher temperatures above T_B. This feature is similar to the case of PZN-9%PT which displays a persisting VV component of CP at high temperatures up to 900 K.[30]

For analyzing the Brillouin doublets corresponding to LA and TA modes, the response function of the damped harmonic oscillator was used, which was approximated by a Lorentzian function since the damping factor of acoustic modes was much smaller than the Brillouin frequency shift. In the fitting process, the Lorentzian function was convoluted by the Gaussian instrumental function of the Fabry-Pérot interferometer. In case of CP, a single Lorentzian function centered at zero was used for the fitting based on the assumption of a single Debye relaxational process for the relevant polarization fluctuations. The spectral response function $S(\nu)$ as a function of the frequency ν for CP is thus expressed as

$$S(\nu) \propto [n(\nu)+1]\frac{2\pi\nu\tau}{1+(2\pi\nu\tau)^2}, \quad (1)$$

where $n(\nu)$ is the Bose-Einstein thermal factor given by

$$n(\nu) = [\exp(h\nu/kT) - 1]^{-1}. \quad (2)$$

In this equation, h and k denote the Planck constant and the Boltzmann constant, respectively. The whole spectrum could be fitted by using a superposition of the above two response functions, and the Brillouin shift, the full width at half maximum (FWHM), and the intensity of the acoustic modes as well as the FWHM and the intensity of CP were derived

from the fitting results as a function of temperature.

The advantage of the present scattering geometry described in Fig. 1 is that the sound velocity can be obtained without the knowledge of the refractive index of the single crystals.[32] The sound velocity V is related to the Brillouin frequency shift ν_B as

$$V = \frac{\lambda_0 \nu_B}{\sqrt{2}}, \tag{3}$$

where λ_0 is the laser wavelength in vacuum. The elastic stiffness coefficients C_{44} and C_{11} are related to the sound velocities according to the following equations:

$$C_{11} = \rho V_L^2, \tag{4}$$

$$C_{44} = \rho V_T^2. \tag{5}$$

In these equations, ρ denotes the density of the crystals and V_L and V_T are longitudinal and transverse sound velocities, respectively. Densities of 8.31 and 8.71 g/cm^3 were used for PZN-4.5%PT and PZN-9%PT, respectively, in order to calculate the above elastic constants.

B. Longitudinal and transverse acoustic modes of PZN-*x*PT

The temperature dependences of ν_B and the FWHM of both LA and TA modes have been obtained and plotted in Figs. 4 and 5, respectively, for PZN-4.5%PT and PZN-9%PT single crystals. T_B of PZN and PZN-9%PT are known to be located in the temperature range between 730 and 750 K, as has been confirmed by the acoustic emission measurements.[19] These values are consistent the previously reported T_B of PZN obtained by the refractive index measurement, which is about 750 K.[7] The Brillouin frequency shift of the LA mode, denoted as ν_B^{LA}, shows an almost linear behavior in the high-temperature range above T_B. The high-temperature slope of ν_B^{LA} of PZN-9%PT is steeper than the case of PZN-4.5%PT. Since no coupling is expected to exist between the acoustic modes and other degrees of freedom related to any phase transformation in this high-temperature range, the temperature dependence of the phonon frequency will be mainly dominated by the lattice anharmonicity.[33] ν_B^{LA} deviates from its high-temperature linearity near T_B in both crystals. Regarding the FWHM, PZN-9%PT shows a change in slope near T_B and begins to increase at ~570 K upon cooling, below which ν_B^{LA} exhibits a significant softening. The FWHM of PZN-4.5%PT begins to increase at about 600 K and shows the onset of the most significant growth at ~500 K with lowering the temperature. It is worth paying attention to the fact that the FWHM of PZN-9%PT also shows a change in the slope at almost the same temperature around 500 K and a substantial increase below it, and these temperatures are very similar to the temperatures at which strong acoustic emission signals were observed in PZN-*x*PT single crystals.[20] ν_B of TA mode (ν_B^{TA}) in Fig. 5 exhibits a similar linear behavior in the high-temperature range, but seems to be less clear due to the more scattered data condition. Regarding the FWHM's of both crystals given in Fig. 5, they show substantial increase below a certain temperature

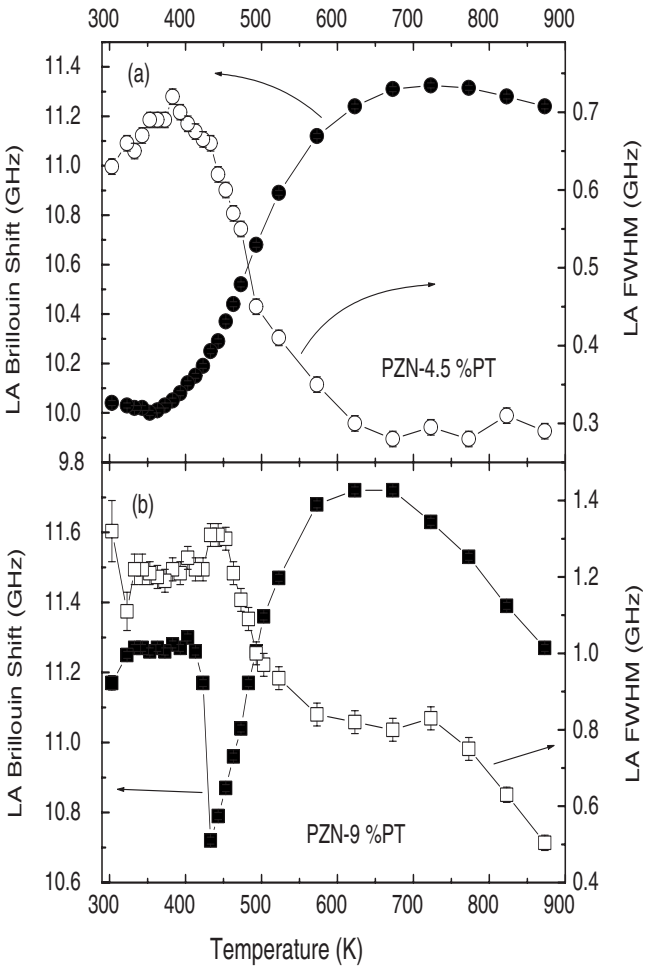

FIG. 4. The Brillouin shift and the FWHM of LA modes of (a) PZN-4.5%PT and (b) PZN-9%PT single crystals as a function of temperature.

around 500 K similar to the case of the LA waves. At low temperatures, ν_B and the FWHM of both modes of PZN-9%PT display abrupt changes at the cubic-to-tetragonal phase transition temperature ($T_{C\text{-}R} \sim 430$ K). In case of PZN-4.5%PT, ν_B exhibits a broad minimum at 360–380 K, while the FWHM shows a broad maximum near the same temperature range, which is consistent with previous study.[34] These results reflect broad phase transition behaviors of PZN-4.5%PT and are similar to the acoustic properties of typical RFEs such as PMN,[35,36] PMT,[37] and lanthanum modified lead zirconate titanate (PLZT).[38]

Figure 6 gives the temperature dependence of the two elastic stiffness coefficients in the pseudocubic coordinate system calculated by using Eqs. (3)–(5). It is found that PZN-4.5%PT is softer than PZN-9%PT single crystals in the whole temperature range. C_{11} and C_{44} of PZN-4.5%PT are 111 and 54 GPa, respectively, at room temperature. These results are similar to those values of [001]-poled PZN-4.5%PT single crystals obtained by the ultrasonic method.[39] In case of PZN-9%PT, C_{11}=144 GPa and C_{44}=62 GPa at room temperature, somewhat higher than those of PZN-4.5%PT single crystals. This large difference might first be considered to be ascribed to the difference in the contribution

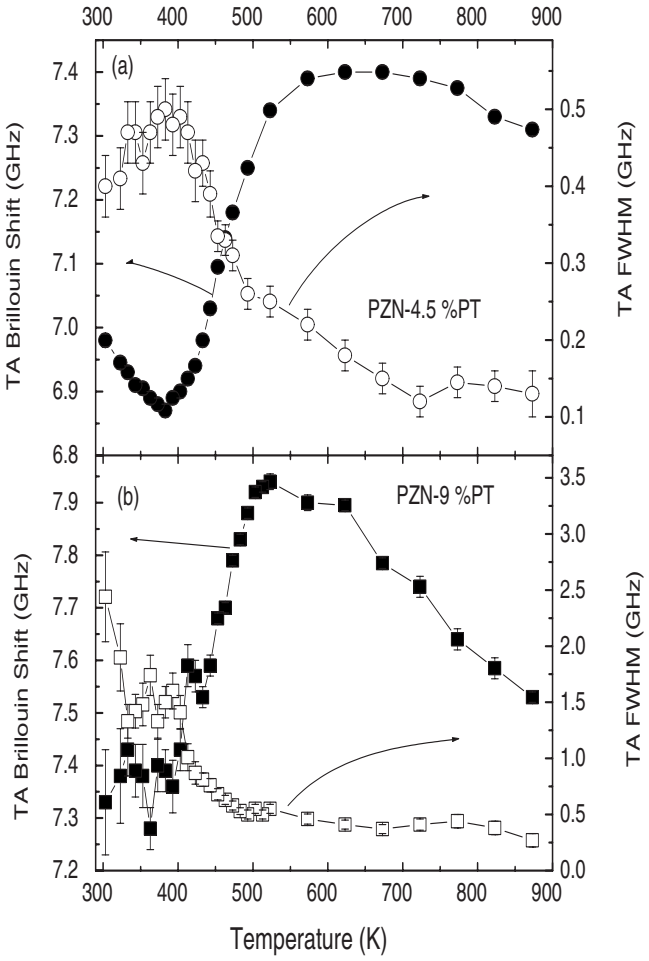

FIG. 5. The Brillouin shift and the FWHM of TA modes of (a) PZN-4.5%PT and (b) PZN-9%PT single crystals as a function of temperature.

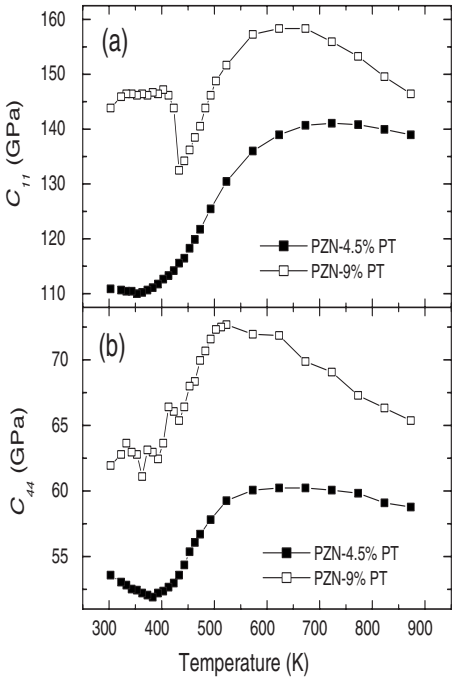

FIG. 6. The temperature dependence of (a) C_{11} and (b) C_{44} of both PZN-4.5%PT and PZN-9%PT crystals as a function of temperature.

from the domain motion and domain walls to the elastic properties of both crystals, because there has been no poling process during the measurement and the domain configuration at room temperature might be different for both crystals because of different PT content. However, the elastic constants of PZN-9%PT sustain higher values than those of PZN-4.5%PT single crystals in the cubic phase where there is no extrinsic contributions from the domain configurations. This indicates that large difference in C_{11} and C_{44} between the two PZN-xPT single crystals may be due to the different PT composition and resultant microstructure. Similar results have been observed in the PMN-42%PT[40] and PMN-30%PT[41] single crystals, where PMN-42%PT located in the tetragonal side of the phase diagram of PMN-xPT shows larger C_{11} compared to that of PMN-33%PT. Another possibility is that there might be some large difference in the frequency dispersion between the two crystals due to different densities of PNRs and their correlation length depending on the PT content.

It is readily recognizable from Figs. 4 and 5 that ν_B^{LA} begins to become softened at higher temperatures than ν_B^{TA} does, implying that the electrostrictive interaction might be anisotropic for the two acoustic modes, i.e., the electrostrictive coupling constant for the LA waves is larger than that for the TA waves near T_B. Similar behaviors were found in PMN investigated by the ultrasonic method.[42] This seems to indicate that the PNRs are more sensitive to LA waves due to higher coupling strength. In order to check whether this behavior is universal or not in RFEs, two archetypal RFEs have been investigated for comparison. The sound velocities of PMN and PMT single crystals have been obtained by using the scattering geometry described in Fig. 1. C_{11} and C_{44} of PMN and PMT have been plotted in Fig. 7. Both C_{11} and C_{44} show linear behaviors in the high-temperature range above T_B. C_{11} deviates from the high-temperature linearity, reaches a maximum near the Burns temperature, and shows a softening below it. In contrast, C_{44} exhibits softening at much lower temperatures. C_{44} of PMN begins to decrease at about 430 K, but exhibits significant softening at and below ~370 K. It was also indicated that a strong dispersion begins to occur in both elastic constants at the same temperature with decreasing temperature,[43] which was ascribed to the onset of the cubic anisotropy. It is also interesting to note that this characteristic temperature is almost the same to that at which Raman spectrum shows a substantial change.[14] In the same way, C_{44} of PMT reaches a maximum at about 380 K, and shows a softening below this temperature. It was also found that the acoustic damping of the LA waves of PMT begins to increase below this temperature upon cooling.[44] These behaviors are very similar to those observed from PZN-4.5%PT and PZN-9%PT single crystals. Therefore, we may suggest that the electrostrictive coupling constant between the LA waves and PNRs is different from that between the TA waves and PNRs. The former is stronger at high temperatures near T_B while the TA waves seem to couple to the PNRs at lower temperatures.

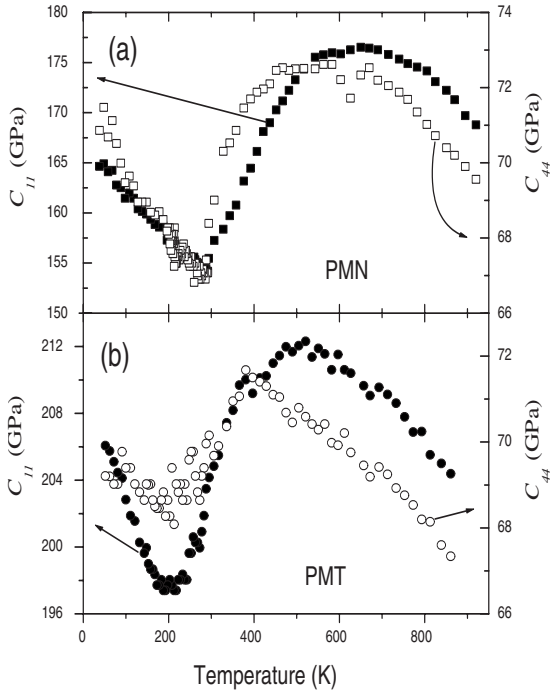

FIG. 7. The temperature dependence of C_{11} and C_{44} of (a) PMN and (b) PMT single crystals as a function of temperature.

C. Central peak behaviors of PZN-*x*PT

CP was fitted by a single Lorentzian centered at zero. Figures 8(a) and 8(b) show temperature dependences of the integrated intensity and the FWHM of CPs (Δ_{CP}), respectively, of PZN-9%PT measured at both polarized and depolarized scattering geometries below 600 K. It was previously shown that the polarized component of the CP persists at high temperatures even above T_B (now shown in this figure).[30] The intensity and the half-width of this VV contribution did not show any significant change with temperature across $T_B \sim 730$ K. In contrast, there was almost no depolarized component of the CP in this high-temperature range above 600 K. Upon cooling, CP exhibits drastic changes. First, the half-width of VV component decreases from ~700 GHz at 595 K down to ~70 GHz near $T_{C\text{-}T}$ while its intensity increases. Second, the VH component begins to appear near 550 K and develops. Below this temperature, the width of this depolarized CP decreases with lowering temperature and its intensity increases with decreasing temperature from 550 K and shows a sudden jump at $T_{C\text{-}T}$. Below ~530 K, both components of CP become narrower significantly indicating marked slowing down of the dynamics of the relevant polarization fluctuations. This is consistent with the fact that all previous Brillouin studies on PZN-*x*PT showed that the VH component of CP appears at temperatures much lower than T_B.[23–26,29] The temperature dependence of the relaxation time τ_R of PNRs estimated from the half-width of CP is plotted in the inset of Fig. 8(b). τ_R estimated from VV component is approximately 0.6 ps above 600 K and increases markedly below this temperature. In addition, τ_R estimated from the width of the VH component exhibits almost the same temperature dependence as that

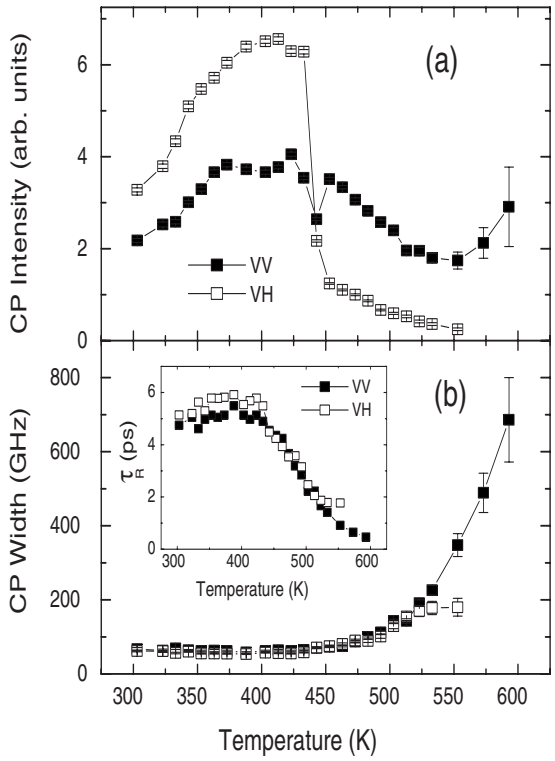

FIG. 8. The temperature dependences of (a) the integrated intensity and (b) the FWHM of CPs of PZN-9%PT single crystals measured at polarized and depolarized scattering geometries. The inset of (b) shows the temperature dependence of relaxation times estimated from the width of polarized and depolarized CPs.

from the VV component below 550 K, which indicates that the VV and VH components of CP are strongly coupled below this temperature. The appearance of the VH component at a certain characteristic temperature indicates restriction of the free reorientation of off-center ions and thus local symmetry lowering in PNRs seems to occur.[14] It is worth noting that the temperature dependences of the half-widths of both components are almost the same below 530 K and that this slowing down is accompanied by the significant softening of the elastic stiffness coefficients, in particular, C_{44}.

The situation is a little bit different in PZN-4.5%PT. Figures 9(a) and 9(b) give temperature dependences of the integrated intensity and the FWHM of CPs, respectively, of PZN-4.5%PT measured at the two scattering geometries. Similar to PZN-9%PT, the polarized component persisted in the high-temperature range above T_B, but the intensity was much weaker compared to PZN-9%PT and reliable fitting procedure was not possible for this high-temperature range. The polarized component was clearly observed below 600 K and Δ_{CP} decreased with lowering temperature. At about 525 K, the depolarized component of CP appears and grows upon cooling. The inset of Fig. 9(b) shows τ_R's of the two CP components. Both relaxation processes exhibit slowing down with decreasing temperature, but τ_R of VH component is larger than that of VV component, which is different from the case of PZN-9%PT. The intensity of both components shows a broad maximum in a wide temperature range in contrast to the case of PZN-9%PT which exhibits significant

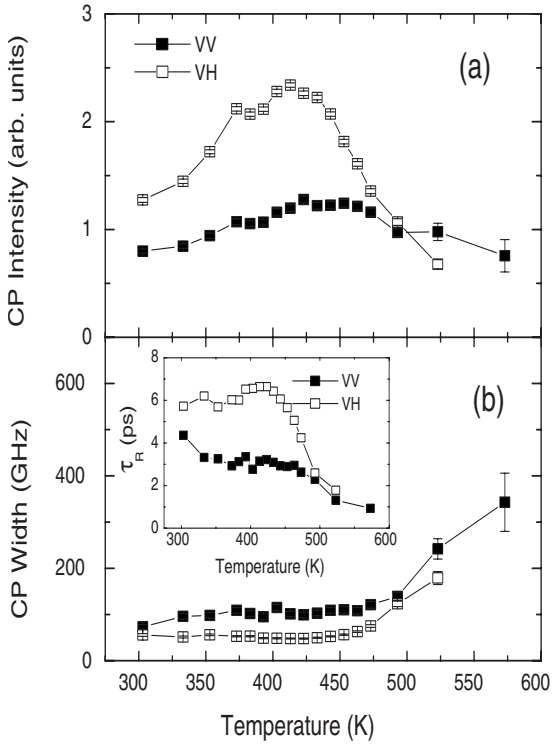

FIG. 9. The temperature dependences of (a) the integrated intensity and (b) the FWHM of CPs of PZN-4.5%PT single crystals measured at polarized and depolarized scattering geometries. The inset of (b) shows the temperature dependence of relaxation times estimated from the width of polarized and depolarized CPs.

changes in the intensity at the phase transition temperature.

The above results suggest some common characteristics of CP behaviors in both PZN-xPT single crystals: (1) the VV component of CP persists even at very high temperatures above T_B; (2) the VH component appears at temperatures around 520–550 K, lower than T_B by ~200 K, which is accompanied by the significant softening of C_{44}; and (3) the relaxation time of both components, related to the relaxation process of the relevant polarization fluctuations, displays dynamic slowing down with decreasing temperature from 550 K toward $T_{C\text{-}T}$ or T_m.

IV. DISCUSSION

The results described in the previous section indicated three characteristic temperatures, i.e., T_B, T_d, and T_m related to the dynamics of RFEs. At high temperatures above T_B, RFEs are in the nonpolar paraelectric phase, which is indistinguishable from the paraelectric phase of normal ferroelectrics. The real part of the complex dielectric constant follows the Curie-Weiss law, and other properties such as the refractive index, the strain, and the unit cell volume show linear behaviors as a function of temperature. The formation of PNRs at T_B has effects on these physical properties as well as acoustic properties via electrostrictive coupling.[9] The correlation between T_B and the anomaly in ν_B of LA mode has been observed in many RFEs, and was used to estimate the temperature dependence of the longest relaxation time of the dielectric distribution function of PMT.[37] This analysis was later extended to the case of PLZT.[38]

Generally, the Landau expression for the free energy F of ferroelectrics can be consisted of three parts: the free energy associated with the order parameter, i.e., the polarization P, the free energy associated with the elastic energy, and finally the coupling term between the order parameter and the strain x. The effective elastic constant $C_{ij}(T)$ of solids which exhibit phase transitions can be described by the Slonczewski-Thomas expression[45]

$$C_{ij} = C_{ij}^{\infty} - \sum_{k,l} \left(\frac{\partial^2 F}{\partial x_i \partial P_k} \right) \left(\frac{\partial^2 F}{\partial P_k \partial P_l} \right)^{-1} \left(\frac{\partial^2 F}{\partial x_j \partial P_l} \right), \qquad (6)$$

where C_{ij}^{∞} is the bare elastic constant independent of P, of which the temperature dependence is determined by the lattice anharmonicity. Since there is no macroscopic spontaneous polarization in the ergodic relaxor phase of RFEs between T_m and T_B, we expect electrostrictive coupling between the order parameter and the strain would dominate the coupling terms in the free energy below T_B. If we include only the electrostrictive interaction (gxP^2) as the lowest coupling term into F where g is the electrostrictive coefficient, the change in the elastic constant owing to this interaction can be expressed[42]

$$\Delta C = C - C^{\infty} = -g^2 \langle P^2 \rangle \chi, \qquad (7)$$

where $\langle P^2 \rangle$ is the mean value of the squared local polarization of PNRs of RFEs and χ is the susceptibility. In the case of the second-order phase transition, $C(T)$ shows a step anomaly at the phase transition temperature since the susceptibility exactly compensates for the change in P^2.[46] In contrast, local polarizations appear at T_B and they gradually grow with decreasing temperature in RFEs.[7] Although the directions of these polarizations are random, their appearance contributes to the decrease of the elastic constant owing to the quadratic nature of the electrostrictive interaction. This decrease would evolve continuously without any abrupt change until the polarization of PNRs is saturated upon cooling. Figures 4 and 7 show that this prediction is indeed observed in LA modes of both PZN-xPT as well as PMN and PMT single crystals, i.e., ν_B^{LA} and C_{11} exhibit continuous softening upon cooling from T_B toward T_m or $T_{C\text{-}R}$.

Regarding CP at high temperatures, only polarized CP appears above T_B, of which the intensity is stronger in PZN-9%PT and much weaker in PZN-4.5%PT. There is no depolarized CP. In this high-temperature range where there is no PNR and where the off-center ions can reorient freely without restriction, rapid 180° reorientations of off-center ions, probably smaller, lighter Nb ions,[47] are expected to contribute to the VV component of CP due to symmetry consideration.[15] It was found that strong CP in the VV geometry was also observed in PMN above 700 K by Raman investigation.[14] The depolarized component of CP appears at much lower temperature at around 520–550 K compared to T_B located in 730–750 K. This additional characteristic temperature T_d (500–550 K) accompanies several unusual changes in the acoustic properties of PZN-4.5%PT and PZN-

9%PT single crystals. That is, T_d is characterized by (i) the appearance of the VH component of CP, (ii) significant decrease in Δ_{CP} of both VV and VH components of CP implying slowing down of the dynamics of PNRs, (iii) the onset of significant softening of c_{44}, and (iv) the increase of the acoustic damping in both LA and TA modes.

Although CPs can be related to several origins in condensed matters, CPs observed in ferroelectrics can arise from soft transverse-optic (TO) phonon, or from some relaxational entities, or from the coupling between them. Since previous studies reported that the TO phonons in PZN and PZN-8%PT are overdamped below T_B,[48,49] the most probable origin of CPs in PZN-xPT would be the relaxational dynamics of PNRs.[23–26,29] The CP dynamics is dominated by the reorientation of the PNRs and the CP width can be used to estimate the approximate relaxation time of the PNRs. It should be pointed out that the temperature at which the depolarized CP appears is lower than T_B by approximately 200 K, consistent with the suggestion that local structural arrangements occur in PNRs at this temperature $\sim T_d$.[15,19] The appearance of CP in the VH geometry at much lower temperatures than T_B indicates that off-diagonal components of the polarizability tensor develop around this temperature. As temperature decreases, the correlation between off-centered ions in PNRs will become enhanced and thus their motion will become more restricted in fewer orientations, gradually losing the symmetric 180° reorientations.[15] Since any local structural transformation in PNRs and the resulting local strain fields can couple to the propagating acoustic waves, the acoustic damping represented by the FWHM of acoustic modes will increase due to the enhancing order-parameter fluctuations. This has indeed been observed from the present study, as the FWHM's of both LA and TA modes exhibit distinct changes in their slopes at ~500 K in both PZN-4.5%PT and PZN-9%PT single crystals (see Figs. 4 and 5). PMN and PMT show very similar characteristics. The FWHM of the LA mode of PMN and PMT begins to increase at approximately 350 and 400 K, respectively, which are much lower than their T_B's.[42,44] Similar results have also been observed in other RFEs such as PMN-xPT single crystals with $x=33\%-35\%$.[50,51] Recent acoustic emission measurements on PZN-xPT with $x=4.5\%-12\%$ showed that strong acoustic activity was observed at almost the same temperature of about 500 K irrespective of the PT content, and this result was attributed to local microscopic phase transition in PNRs embedded in a nonpolar cubic matrix based on the fact that the acoustic emission signal is normally very sensitive to small structural changes.[20] Considering that significant changes in the acoustic damping and the strong acoustic activity in addition to the substantial change in the Raman spectrum of PZN-4.5%PT[16] occur at almost the same temperature, it can be safely concluded that both phenomena share the same microscopic origin related to some local structural changes in PNRs.

The exact nature of this local structural transformation in PNRs cannot be clearly revealed from the present Brillouin study, and more refined microscopic probe and analysis are necessary for resolving it. However, some possible candidate for the changes occurring in PNRs at T_d might be suggested based on the symmetry considerations. In the cubic symmetry, there are three eigenvalues for the elastic constant matrix, that is, $C_{11}+2C_{12}$, $C_{11}-C_{12}$, and C_{44}.[52] $C_{11}+2C_{12}$ corresponds to hydrostatic deformation while $C_{11}-C_{12}$ and C_{44} are related to the acoustic instabilities of the tetragonal and/or orthorhombic and rhombohedral (or trigonal) deformations, respectively. A phase transition associated with a uniform deformation should accompany vanishingly small elastic constant and sound velocity corresponding to that deformation. The most noteworthy result of this study is that, with decreasing temperature, C_{44}'s of all the investigated RFEs exhibit the onset of softening at temperatures around T_d much lower than T_B, the temperature for the formation of PNRs. Acoustic damping, desymmetrization of the polarization tensor represented by the appearance of the depolarized CP, and generation of strong acoustic emission signals accompany the onset of the softening of C_{44}. This might suggest that the nature of the local structural transformation occurring at T_d and being enhanced upon further cooling is rhombohedral. The gradual softening of C_{44} would then be correlated to the growth of the rhombohedral PNRs in the nonpolar cubic matrix. This onset of local transformation in PNRs may enhance the coupling between the TA waves and PNRs and thus be the origin of the anisotropic electrostrictive interaction between PNRs and the two acoustic waves. This suggestion is consistent with the results of previous neutron scattering studies on PZN, which showed that the rhombohedral phase appears at about 550 K,[22] and that the local structure of PNRs at low temperatures is rhombohedral.[53]

From the above results and discussions, it becomes obvious that the coupling between the dynamics of PNRs and acoustic modes, in particular, TA waves, become substantial at T_d. In addition, the increase of the intensity of CP and their narrowing in width signify that the density of PNRs and interactions between them begin to grow at this temperature. Therefore, it may be indicated that T_d is a characteristic temperature at which long-lived PNRs begins to form via local phase transformation into, probably, rhombohedral symmetry, inducing local strain fields. According to recent neutron scattering studies on PMN, a local phase transformation at T_d(~370 K) has been suggested and interpreted in terms of the role of the cubic anisotropy and the random-field-driven phase transition.[17] These strain fields around PNRs will be coupled to the acoustic modes resulting in the changes of acoustic properties, in particular, substantial acoustic damping observed in this study. Upon further cooling, PZN-9%PT shows a clear structural phase transition at $T_{C\text{-}R}$ exhibiting discontinuous changes in acoustic properties and thus long-range ferroelectric order is realized due to the high PT content, while PZN-4.5% displays broad acoustic behaviors typical in RFEs during the diffuse phase transition. The PT content would affect the strength of the random fields as well as the percolation condition of PNRs in PZN-xPT.

Finally, it is worth comparing the present results with acoustic properties of seemingly very different relaxor systems, $KTa_{1-x}Nb_xO_3$ (KTN).[54] From this previous ultrasonic study on KTN single crystals with four different Nb concentrations, it was found that a significant softening of C_{11} and C_{44} and a substantial increase in their corresponding attenuations occur in the temperature range above the phase tran-

sition temperature where PNRs appear. Moreover, C_{44} was observed to soften closer to the transition temperature than C_{11}. All these results are very similar to those of PZN-xPT obtained in the present study. It should thus be pointed out that more systematic and thorough investigations into the polarization-strain coupling and associated phenomena in different relaxor systems are highly desirable in order to identify general features of relaxor dynamics.[55]

V. SUMMARY AND CONCLUSION

The temperature dependence of acoustic properties of PZN-xPT with $x=0.045$ and 0.09 single crystals has been investigated in a wide temperature range by Brillouin light scattering. Temperature dependences of the acoustic modes and CP of these relaxor-based complex perovskites revealed three characteristic temperature regions divided by two characteristic temperatures, T_B and T_d, which can be correlated to the temperature evolution of the dynamics of PNRs.

(1) Above T_B, the acoustic phonons showed a linearly decreasing behavior with increasing temperature reflecting normal lattice anharmonicity. The quasielastic CP is polarized with a weak intensity without any depolarized component. The Brillouin frequency shift of the LA waves shows a mild change in slope at the temperature of the formation of PNRs, T_B, well correlating with other unusual phenomena such as the deviation of the dielectric constant, the refractive index, the strain, from high-temperature linear behaviors, etc. Both C_{11} and C_{44} display broad maxima and gradual softening upon cooling from T_B as the electrostrictive interaction between PNRs and the acoustic waves is enhanced with lowering temperature. However, C_{11} and C_{44} show different temperature dependences, i.e., C_{11} exhibits the onset of softening at higher temperatures than C_{44} does indicating anisotropic electrostrictive coupling between PNRs and the two acoustic waves.

(2) At a certain temperature of T_d located below T_B by more than 200 K, depolarized CP began to appear concomitant with the drastic softening of C_{44} upon cooling from this temperature. In addition, the onset of substantial increase of the acoustic damping of both acoustic waves at T_d could be seen from the temperature dependence of FWHM of Brillouin doublets suggesting enhanced electrostrictive coupling of the strain to the square of the local polarization of PNRs due to local structural changes occurring in PNRs. Based on symmetry considerations, it is suggested that the local transformation occurring in PNRs might be rhombohedral. With further cooling from T_d, the CP width decreased and the relaxation time of the relevant polarization fluctuations increased reflecting the slowing down of the dynamics related to the reorientation of PNRs.

The present Brillouin-scattering study suggests a clear experimental evidence of the existence of the intermediate characteristic temperature T_d located in 500–550 K in PZN-xPT at which significant changes in acoustic properties are brought about, and this temperature might indicate that long-lived PNRs and associated local strain fields are formed not at T_B but at a much lower temperature $T_d=500-550$ K. This suggestion is further supported by the fact that strong acoustic emission signals, diffuse neutron scattering, and substantial changes in the Raman spectrum appear at almost the same temperature. Considering almost the same temperature characteristics of C_{11} and C_{44} and related acoustic damping factors observed from two representative RFEs, PMN and PMT, this conclusion might be considered as being more common properties of RFEs and the dynamics of PNRs rather than being restricted to only PZN-xPT single crystals.

ACKNOWLEDGMENTS

The authors are thankful to C. D. Feng (Shanghai Institute of Ceramics) for providing us with PZN-xPT single crystals, and also appreciate S. G. Lushnikov (A. F. Ioffe Physico-Technical Institute of Russian Academy of Sciences) for helpful discussions and supplying the Brillouin data of PMN and PMT. This work was supported in part by the Korea Research Foundation Grant funded by the Korean Government (MOEHRD, Basic Research Promotion Fund) (KRF-2006-331-C00088).

*hwangko@hallym.ac.kr
†kojima@bk.tsukuba.ac.jp

[1] L. E. Cross, Ferroelectrics **76**, 241 (1987).
[2] G. Burns and F. H. Dacol, Ferroelectrics **104**, 25 (1990).
[3] S.-E. Park, and T. R. Shrout, J. Appl. Phys. **82**, 1804 (1997).
[4] D. Viehland, S. J. Jang, L. E. Cross, and M. Wuttig, J. Appl. Phys. **68**, 2916 (1990).
[5] A. E. Glazounov and A. K. Tagantsev, Appl. Phys. Lett. **73**, 856 (1998).
[6] N. de Mathan, E. Husson, G. Calvarin, J. R. Gavarri, A. W. Hewat, and A. Morell, J. Phys.: Condens. Matter **3**, 8159 (1991).
[7] G. Burns and F. H. Dacol, Solid State Commun. **48**, 853 (1983).
[8] W. Kleemann, J. Mater. Sci. **41**, 129 (2006).
[9] For a review, see A. A. Bokov and Z.-G. Ye, J. Mater. Sci. **41**, 313 (2006).
[10] V. Westphal, W. Kleemann, and M. D. Glinchuk, Phys. Rev. Lett. **68**, 847 (1992).
[11] R. Pirc and R. Blinc, Phys. Rev. B **60**, 13470 (1999).
[12] B. P. Burton, E. Cockayne, and U. V. Waghmare, Phys. Rev. B **72**, 064113 (2005).
[13] J.-H. Ko, S. Kojima, A. A. Bokov, and Z.-G. Ye, Appl. Phys. Lett. **91**, 252909 (2007).
[14] O. Svitelskiy, J. Toulouse, G. Yong, and Z.-G. Ye, Phys. Rev. B **68**, 104107 (2003).
[15] J. Toulouse, F. Jiang, O. Svitelskiy, W. Chen, and Z.-G. Ye, Phys. Rev. B **72**, 184106 (2005).
[16] O. Svitelskiy, D. La-Orauttapong, J. Toulouse, W. Chen, and Z.-G. Ye, Phys. Rev. B **72**, 172106 (2005).
[17] S. N. Gvasaliya, B. Roessli, R. A. Cowley, P. Huber, and S. G.

Lushnikov, J. Phys.: Condens. Matter **17**, 4343 (2005).
[18] S. N. Gvasaliya, B. Roessli, R. A. Cowley, S. Kojima, and S. G. Lushnikov, J. Phys.: Condens. Matter **19**, 016219 (2007).
[19] E. Dul'kin, M. Roth, P.-E. Janolin, and B. Dkhil, Phys. Rev. B **73**, 012102 (2006).
[20] M. Roth, E. Mojaev, E. Dul'kin, P. Gemeiner, and B. Dkhil, Phys. Rev. Lett. **98**, 265701 (2007).
[21] G. Xu, Z. Zhong, H. Hiraka, and G. Shirane, Phys. Rev. B **70**, 174109 (2004).
[22] K. Fujishiro, T. Iwase, Y. Uesu, Y. Yamada, B. Dkhil, J. Kiat, S. Mori, and N. Yamamoto, J. Phys. Soc. Jpn. **69**, 2331 (2000).
[23] M. H. Kuok, S. C. Ng, H. J. Fan, M. Iwata, and Y. Ishibashi, Solid State Commun. **118**, 169 (2001).
[24] M. H. Kuok, S. C. Ng, H. J. Fan, M. Iwata, and Y. Ishibashi, Appl. Phys. Lett. **78**, 1727 (2001).
[25] Y. Gorouya, Y. Tsujimi, Y. Yamashita, T. Ifukube, and T. Yagi, Ferroelectrics **266**, 165 (2002).
[26] Y. Gorouya, Y. Tsujimi, M. Iwata, and Y. Yagi, Appl. Phys. Lett. **83**, 1358 (2003).
[27] D. H. Kim, J.-H. Ko, C. D. Feng, and S. Kojima, Appl. Phys. Lett. **87**, 072908 (2005).
[28] D. H. Kim, J.-H. Ko, C. D. Feng, and S. Kojima, J. Appl. Phys. **98**, 044106 (2005).
[29] Y. Nakata, Y. Tsujimi, K. Katsuraya, M. Iwata, and T. Yagi, Appl. Phys. Lett. **89**, 022903 (2006).
[30] J.-H. Ko, D. H. Kim, and S. Kojima, Appl. Phys. Lett. **90**, 112904 (2007).
[31] R. Vacher and L. Boyer, Phys. Rev. B **6**, 639 (1972).
[32] J. M. Vaughan, *The Fabry-Perot Interferometer* (The Adam Hilger, Bristol, 1989), p. 348.
[33] E. Courtens, R. Vacher, and Y. Dagorn, Phys. Rev. B **33**, 7625 (1986).
[34] J.-H. Ko, D. H. Kim, S. Kojima, W. Chen, and Z.-G. Ye, J. Appl. Phys. **100**, 066106 (2006).
[35] R. Laiho, S. Lushnikov, and I. Siny, Ferroelectrics **125**, 493 (1992).
[36] S. G. Lushnikov, J.-H. Ko, and S. Kojima, Appl. Phys. Lett. **84**, 4798 (2004).
[37] J.-H. Ko, S. Kojima, and S. G. Lushnikov, Appl. Phys. Lett. **82**, 4128 (2003).
[38] G. Shabbir, J.-H. Ko, S. Kojima, and Q.-R. Yin, Appl. Phys. Lett. **82**, 4696 (2003).
[39] J. H. Yin, B. Jiang, and W. Cao, IEEE Trans. Ultrason. Ferroelectr. Freq. Control **47**, 285 (2000).
[40] H. Cao, V. H. Schmidt, R. Zhang, W. Cao, and H. Luo, J. Appl. Phys. **96**, 549 (2004).
[41] R. Zhang, W. Jiang, B. Jiang, and W. Cao, *Fundamental Physics of Ferroelectrics* (American Institute of Physics, New York, 2002), p. 188.
[42] G. A. Smolenskii, N. K. Yushin, and S. I. Smirnov, Sov. Phys. Solid State **27**, 492 (1985).
[43] S. G. Lushnikov (unpublished).
[44] S. G. Lushnikov, A. I. Fedoseev, S. N. Gvasaliya, J.-H. Ko, and S. Kojima, J. Phys.: Condens. Matter **19**, 496206 (2007).
[45] J. C. Slonczewski and H. Thomas, Phys. Rev. B **1**, 3599 (1970).
[46] W. Rehwald, Adv. Phys. **22**, 721 (1973).
[47] B. E. Vugmeister, Phys. Rev. B **73**, 174117 (2006).
[48] P. M. Gehring, S.-E. Park, and G. Shirane, Phys. Rev. Lett. **84**, 5216 (2000).
[49] P. M. Gehring, S.-E. Park, and G. Shirane, Phys. Rev. B **63**, 224109 (2001).
[50] F. M. Jiang and S. Kojima, Phys. Rev. B **62**, 8572 (2000).
[51] G. Shabbir and S. Kojima, Appl. Phys. Lett. **91**, 062911 (2007).
[52] R. A. Cowley, Phys. Rev. B **13**, 4877 (1976).
[53] I.-K. Jeong and J. K. Lee, Appl. Phys. Lett. **88**, 262905 (2006).
[54] L. A. Knauss, X. M. Wang, and J. Toulouse, Phys. Rev. B **52**, 13261 (1995).
[55] J. Toulouse, D. La-Orauttapong, and O. Svitelskiy, Ferroelectrics **302**, 271 (2004).